Advances in numerical simulations of ion cyclotron heating of non-Maxwellian plasmas

M. Brambilla and R. Bilato

Max-Planck Institut für Plasmaphysik – EURATOM Association – Garching, Germany

E-mail: roberto.bilato@ipp.mpg.de

Abstract. Coupling the full-wave solver TORIC (Plasma Phys. Contr. Fusion **41**, 1, (1999)) and the bounce-averaged quasilinear Fokker-Planck solver SSFPQL (Nucl. Fusion **34**, 1121, (1994)) allows to determine the suprathermal ion populations produced by ion cyclotron heating of tokamak plasmas, while taking into account their effects on wave propagation and absorption. By using new numerical methods for the evaluation of the coefficients of the wave equations in non-Maxwellian plasmas and the transmission of data between TORIC and SSFPQL, the interface between the two codes has been made very efficient and accurate. As an example, we have re–analysed a minority heating scenario in the ASDEX Upgrade tokamak. The results illustrate the differences between the quasilinear evolution of fundamental and first harmonic ion cyclotron heating due to the fact that the latter is a finite Larmor radius effect. They also suggest that the main missing element for fully satisfactory self-consistent simulations of ion cyclotron experiments in toroidal devices is the absence of a detailed model for the losses of suprathermal ions due, for example, to interactions with low frequency turbulence or magnetohydrodynamic instabilities.

PACS numbers: 52.35.Hr, 52.50.Qt, 52.55.Fa, 52.65.-y

1. Introduction

The numerical simulation of radio-frequency (RF) heating and current drive in fusion plasmas has reached the state in which self-consistent solutions can be achieved by iterating between a solver of the wave equations and a solver of the quasilinear kinetic equation. In this paper we present a tool which implements this iteration for waves in the ion cyclotron (IC) range of frequencies, the package TORIC-SSFPQL [1].

TORIC [2, 3] solves Maxwell's equations in axisymmetric toroidal plasmas, assuming a constitutive relation (linear relation between high-frequency field and high-frequency plasma current) obtained from the linearized Vlasov equation by expanding the field in toroidal and poloidal Fourier components. The model includes propagation and damping of externally launched fast waves (FW), and of ion Bernstein (IBW) and ion cyclotron waves excited by linear mode conversion (LMC) near ion-ion resonances. The absorption channels are fundamental and first harmonic IC heating of ions, and Landau and transit time damping of electrons. The integral constitutive relation is put into differential form in the radial direction by assuming wavelengths large compared to the thermal ion Larmor radius; large Larmor radius corrections, however, are taken into account to adequately describe IBWs [4]. Optionally, damping of the FW at higher IC harmonics can be simulated, although not simultaneously with mode conversion [5]. Recent applications of the TORIC code can be found in [6].

The Fokker-Planck quasilinear solver SSFPQL [7] evaluates the steady-state quasilinear distribution function of ions heated at the fundamental and first harmonic IC resonance by balancing the bounce-averaged quasilinear operator (QLO) with the linearized collision operator describing collisions with a Maxwellian background plasma. The solution is obtained as a truncated series in Legendre polynomials. A special Bessel function identity is used to guarantee that the truncated expansion of the QLO remains positive definite up to a sufficiently high energy. This approach does not allow to deal with the most energetic ions generated by IC resonances, or to follow transients when the hf power is modulated in time, or switched on and off. On the other hand, it is very fast and easy to implement. With some further limitations to be discussed below, most of them common to all models based on surface averaging, the information provided by SSFPQL on the radial profiles of the quasilinear distribution functions of ICRF heated plasmas and on the collisional exchanges between the heated and background ions are fully adequate for most purposes.

The TORIC-SSFPQL package is not the first effort to combine a model for wave propagation and absorption with a model for the evolution of the ion distributions. The PION code [8], although using a very simple model for the power absorption profiles and a one-dimensional Fokker-Planck solver 'corrected' for anisotropy and other effects, has proven to be an excellent interpretative tool [9, 10]. Dumont et al. [11] have explored the consequences of suprathermal populations on wave propagation and absorption in a slab model of toroidal plasmas. The most advanced self-consistent simulations in toroidal geometry have been recently made by combining the full-wave toroidal code AORSA

with the quasilinear-Fokker-Planck code CQL3D [12, 13]. It is also worth mentioning that the importance of high energy ions in fusion plasmas [14, 15] has stimulated a considerable effort to determine the evolution of the most energetic populations created by IC resonant interactions. Since these ions tend to be trapped on banana or non-standard orbits making large radial excursions which do not justify bounce-averaging, orbit following and Monte Carlo methods have been developed [16, 17], and applied for self-consistent simulations [18, 19]. The Monte Carlo approach, however, is really efficient only in the high-energy domain. Deviations from local thermal equilibrium, on the other hand, influence wave propagation most in the intermediate energy range, where Monte Carlo simulations are relatively slow and noisy. In this range bounce-averaging is justified, and has the advantage of producing directly smooth distribution functions, as needed by wave solvers.

A first attempt to iterate between TORIC and SSFPQL was presented in [1]. In that work, the distribution function of minority ions was approximated by the superposition of two anisotropic Maxwellians, representing the thermal part and the suprathermal tail, respectively, whose parameters where fitted as well as possible to the solution evaluated by SSFPQL following the classical solution of Stix [20]. With this representation of the quasilinear distribution function the coefficients of the wave equations can be reevaluated analytically, making the iteration of TORIC very simple. Although capturing the main features of self-consistency, this approach was limited to minority heating scenarios, and a quantitative estimate of the accuracy was not possible. To combine TORIC and SSFPQL for general IC heating scenarios we have now made a number of improvements to both codes, and implemented an efficient interface between them. These developments are the object of the present paper. We begin in section 2 by briefly recalling the main features of SSFPQL. In sections 3 and 4 we then describe the modifications which have been made to make it suitable for coupling with TORIC. They include: a 'source' to ensure compatibility of the linearized collisional operator with a steady state with different ion and electron temperatures; accounting for the contribution of the r.h. circular field component E_- to the QL diffusion coefficient [8]; and optional extensions to take into account toroidal trapping and broadening of the power deposition profiles by the finite radial width of 'banana' orbits.

In section 5 we recall how the coefficients of the wave equations have to be modified when the distribution functions are not Maxwellians. In these coefficients, the familiar Plasma Dispersion function [21] of the Maxwellian case has to be replaced by singular integrals over moments of the distribution functions. An efficient and accurate numerical scheme for the evaluation of these integrals has been implemented by expanding an idea of Valeo [22]; it is explained in section 6. In the same section we also briefly present the interface between SSFPQL and TORIC, designed to be as simple and robust as possible. Section 7 presents some applications of the package, followed by conclusions in section 8.

2. The steady-state Fokker-Planck Quasilinear solver SSFPQL

The code SSFPQL solves the steady-state quasilinear kinetic equation for IC heated ions

$$0 = \left(\frac{\partial F_i}{\partial t}\right)_{coll} + \left(\frac{\partial F_i}{\partial t}\right)_{QL} + S_i \tag{1}$$

in which energy losses to the background plasma described by the linearized collisional operator balance the gains described by the quasilinear operator and, if required, a source or sink S_i.

1) The linearized collisional operator describing test particles colliding with a background Maxwellian plasma is

$$\frac{1}{\nu_i}\left(\frac{\partial F_i}{\partial t}\right)_{coll} = \frac{1}{v^2}\frac{\partial}{\partial v}\left[v^2\left(\frac{\Psi_c(v)}{2v}\frac{\partial F_i}{\partial v} + \Psi_\tau(v)F_i\right)\right] + \frac{\Theta_c(v)}{2v^3}\frac{\partial}{\partial \mu}\left((1-\mu^2)\frac{\partial F_i}{\partial \mu}\right) \tag{2}$$

Here v is normalized to $v_{th\alpha} = (2T_\alpha/m_\alpha)^{1/2}$, the thermal speed of species α in the background plasma, and $\mu = v_\parallel/v$ is the cosine of the velocity pitch angle. The coefficients are defined as

$$\begin{gathered}\Psi_c(v) = \sum_\beta \frac{\nu^{i/\beta}}{\nu_i}\Psi(\gamma_{i\beta}v) \qquad \Psi_\tau(v) = \sum_\beta \frac{\nu^{i/\beta}}{\nu_i}\frac{T_i}{T_\beta}\Psi(\gamma_{i\beta}v) \\ \Theta_c(v) = \sum_\beta \frac{\nu^{i/\beta}}{\nu_i}\Theta(\gamma_{i\beta}v)\end{gathered} \tag{3}$$

with $\gamma_{i\beta} = v_{thi}/v_{th\beta}$ and

$$\begin{aligned}\Psi(u_\beta) &= \frac{\Phi(u_\beta)}{u_\beta^2} \\ \Theta(u_\beta) &= \frac{1}{2u_\beta}\frac{d\Phi}{du_\beta} + \left(u_\beta^2 - \frac{1}{2}\right)\frac{\Phi(u_\beta)}{u_\beta^2}\end{aligned} \tag{4}$$

with $u_\beta = \gamma_{i\beta}\, v$, in terms of the basic function

$$\Phi(u_\beta) = \frac{4}{\sqrt{\pi}}\int_0^{u_\beta} u^2\, e^{-u^2}\, du = -\frac{2}{\sqrt{\pi}}u_\beta\, e^{-u_\beta^2} + \mathrm{Erf}\,(u_\beta) \tag{5}$$

In these expressions

$$\nu_{i\beta} = \frac{4\pi\, Z_i^2 Z_\beta^2 e^4\, n_\beta \Lambda^{\alpha\beta}}{m_i^2 v_{thi}^3} \qquad \nu_i = \sum_\beta \nu_{i\beta} \tag{6}$$

(ν_i actually cancels out from the equations).

As mentioned in the Introduction, the distribution function is expanded as a truncated series in Legendre polynomials of the velocity pitch angle,

$$F_i(v,\mu,t) = \sum_{n=0}^{N} F_n^i(v,t)\, P_n(\mu) \tag{7}$$

The linearized collisional operator is diagonal in this representation:

$$\frac{1}{\nu_i}\left(\frac{\partial F_n^i}{\partial t}\right)_{coll} = \frac{1}{v^2}\frac{d}{dv}\left[v^2\left(\frac{\Psi_c(v)}{2v}\frac{dF_n^i}{dv} + \Psi_\tau(v)F_n^i\right)\right] - n(n+1)\,\frac{\Theta_c(v)}{2v^3}\,F_n^i \tag{8}$$

2) The quasilinear operator describing ion cyclotron resonant interactions is approximated as

$$\left(\frac{\partial F_i}{\partial t}\right)_{QL} = \frac{1}{v_\perp}\frac{\partial}{\partial v_\perp}\left(v_\perp\, D_{\rm ql}^p(v_\perp)\,\frac{\partial F_i}{\partial v_\perp}\right) \tag{9}$$

with the following expression for the quasilinear diffusion coefficient (QLDC) $D_{\rm ql}^p$ for heating at the p-th harmonic

$$D_{\rm ql}^p = \frac{Z^2e^2}{2m^2}\,D_0\sum_{m,n}|E_+|^2\Big|J_{p-1}(\xi_\perp w) + \lambda_{\rm P}\,J_{p+1}(\xi_\perp w)\Big|^2 \tag{10}$$

($p=1$ for fundamental, $p=2$ for harmonic IC heating) where $\xi_\perp = k_\perp v_{thi}/\Omega_{ci}$ and $w = v_\perp/v_{thi}$, and

$$\lambda_P = \left(\frac{E_-}{E_+}\right)_{\rm res} \simeq \left(\frac{n_\parallel^2 - R}{n_\parallel^2 - L}\right)_{\rm res} \tag{11}$$

The sum in eqn (10) is over poloidal and toroidal modes. The perpendicular wavevector $k_\perp$ of the fast wave and the field amplitudes $E_\pm$ of the circularly polarized electric field components are to be taken at the resonance point separately for each Fourier component. In principle, $D_0 \equiv 1$. On each magnetic surface, however, D_0 is reevaluated by imposing that the h.f. power absorbed W_M should be identical to the surface-averaged power per unit volume gained by the ions according to TORIC when evaluated with the same distribution function. In the present context, this is more than simple convenience, as will be discussed below.

Recalling $u = v\mu$, $w = v\sqrt{1-\mu^2}$, the QLO (9) can be rewritten in spherical coordinates as

$$\begin{aligned}\frac{1}{\nu_i}\left(\frac{\partial F_i}{\partial t}\right)_{QL} =& \frac{1-\mu^2}{v^2}\frac{\partial}{\partial v}\left[v\,D_{\rm ql}(\xi_\perp w)\,\left(v\frac{\partial F_i}{\partial v} - \mu\frac{\partial F_i}{\partial \mu}\right)\right] \\ &- \frac{1}{v^2}\frac{\partial}{\partial \mu}\left[\mu(1-\mu^2)\,D_{\rm ql}(\xi_\perp w)\,\left(v\frac{\partial F_i}{\partial v} - \mu\frac{\partial F_i}{\partial \mu}\right)\right]\end{aligned} \tag{12}$$

Because of the anisotropy of the QLDC, in the Legendre representation this operator is not even approximately diagonal. As a consequence, achieving convergence of the expansion (7) to a positive definite distribution function requires some care. The simplest approach, consisting in developing the squared Bessel function in powers of the argument, and evaluating the coefficients of the Legendre expansion term by term, although analitycally straightforward, converges too slowly to be of any practical use ‡

‡ This was already well-known to Killeen and coworkers, who abandoned the Legendre expansion technique originally used for mirror plasmas [23] to develop the first FP kinetic solver including the IC quasilinear operator discretized in two velocity coordinates, in order to circumvent this problem [24]. As recently as 1997, the convergence of the Legendre expansion has been studied in the limit of negligible ion Larmor radius, $|J_0(k_\perp v_\perp/\Omega_{ci})|^2 = 1$ and, not surprisingly, has been found unsatisfactory [25].

Instead, we use the multiplication theorem of Bessel functions to develop

$$J_p\left(\xi_\perp v\sqrt{1-\mu^2}\right) = (1-\mu^2)^{p/2}\sum_{k=0}^{\infty}\frac{\mu^{2k}}{k!}\left(\frac{\xi_\perp v}{2}\right)^k J_{p+k}(\xi_\perp v) \tag{13}$$

Substituting (7) into (12) and using this identity, we obtain for each n

$$\begin{aligned}\frac{1}{\nu_i}\left(\frac{\partial F_n^i}{\partial t}\right)_{QL} = \left(n+\frac{1}{2}\right)\sum_m\Bigg\{&\frac{1}{v^2}\frac{d}{dv}\left(v^2\mathcal{D}_{00}^p(n,m,\,v)\frac{dF_m^i}{dv}\right)\\ &-\frac{1}{v^2}\frac{d}{dv}\Big(v\,\mathcal{D}_{01}^p(n,m,\,v)\,F_m^i\Big)+\frac{\mathcal{D}_{10}^p(n,m,\,v)}{v}\frac{dF_m^i}{dv}-\frac{\mathcal{D}_{11}^p(n,m,\,v)}{v^2}F_m^i\Bigg\}\end{aligned} \tag{14}$$

with coefficients

$$\begin{aligned}\mathcal{D}_{ij}^p(n,m,\,v) = D_0\sum_{k=0}^{\infty}\Big[&Q_{ij}^{p-1,k}(n,m)\,\mathcal{J}_k^{p-1,p-1}(\xi_\perp v)+2\mathrm{Re}(\lambda_P)\,Q_{ij}^{p,k}(n,m)\,\mathcal{J}_k^{p-1,p+1}(\xi_\perp v)\\ &+|\lambda_P|^2 Q_{ij}^{p+1,k}(n,m)\,\mathcal{J}_k^{p+1,p+1}(\xi_\perp v)\Big]\end{aligned} \tag{15}$$

where

$$\mathcal{J}_k^{p,q}(\xi_\perp v) = \left(\frac{\xi_\perp v}{2}\right)^k\sum_{k'=0}^{k}\frac{1}{k'!(k-k')!}J_{p+k'}(\xi_\perp v)J_{q+k-k'}(\xi_\perp v) \tag{16}$$

and the quantities $Q_{ij}^{p,k}(n,m)$ are integrals over products of two Legendre polynomials weighted with powers of μ^2 and $1-\mu^2$ §

$$\begin{aligned}Q_{00}^{p,k}(n,m) &= \int_{-1}^{+1}P_n(\mu)\,(1-\mu^2)^{1+p}\,\mu^{2k}\,P_m(\mu)\,d\mu\\ Q_{01}^{p,k}(n,m) &= \int_{-1}^{+1}P_n(\mu)\,(1-\mu^2)^{1+p}\,\mu^{2k}\left(\mu\frac{\partial P_m}{\partial\mu}\right)d\mu\\ Q_{10}^{p,k}(n,m) &= \int_{-1}^{+1}\left(\mu\frac{\partial P_n}{\partial\mu}\right)(1-\mu^2)^{1+p}\,\mu^{2k}\,P_m(\mu)\,d\mu\\ Q_{11}^{p,k}(n,m) &= \int_{-1}^{+1}\left(\mu\frac{\partial P_n}{\partial\mu}\right)(1-\mu^2)^{1+p}\,\mu^{2k}\left(\mu\frac{\partial P_m}{\partial\mu}\right)d\mu\end{aligned} \tag{17}$$

These integrals can be evaluated iteratively using the recurrence relations of the Legendre polynomials. These relations are presented in Appendix 1A.

3) Presently implemented in SSFPQL is an isotropic source term which allows background steady-states in which different charged species have different temperatures; it will be discussed in the next section. A more general source term describing neutral beam injection is in preparation.

§ For simplicity, here the spectrum of toroidal modes excited by the antenna is assumed symmetric, so that the quasilinear distribution functions is symmetric in $v_\parallel$, except for the neoclassic effect due to finite banana orbits mentioned in section 4. SSFPQL, however, allows also for non-symmetric distribution functions, as occurring when the antenna excitation is asymmetric, and, more importantly, when IC heating is performed together with unbalanced neutral beam injection.

3. A discussion of the SSFPQL model

In this and the next section we describe the most important improvements that had to be made to the SSFPQL code in view of coupling it with TORIC. We also briefly discuss the limitations of the SSFPQL model, while at the same time trying to make it plausible that the code is fully adequate for self-consistent simulations of IC heating in tokamaks. For this purpose, we will have to recall some aspects of the relations between the properties of the quasilinear distribution functions and the coefficients of the wave equations in the IC range of frequencies which are well-known, but are, nevertheless, occasionally overlooked in this context.

1) In the absence of RF heating, the linearized collisional operator (2) admits a steady-state solution only if all charged species have the same temperature, a situation seldom occurring in practice. Ideally, one would like to be able to evolve the solution of the kinetic equation itself to reproduce the observed temperature profiles. In the absence of a realistic model for energy losses, however, this is manifestly impossible. Instead, we take the profiles as given, either from experiment or from a transport code, and we add to eqn (2) the source (or sink) required to make them the steady-state solution. A simple calculation shows that the appropriate source for species i is, on each magnetic surface,

$$S_i(v) = \nu_i \sum_\beta \frac{\nu^{i/\beta}}{\nu_i}\Big(\frac{T_i}{T_\beta} - 1\Big)\Big(\frac{4\gamma_{i\beta}}{\sqrt{\pi}}\, e^{-u_\beta^2} - 2v\,\Psi(u_\beta)\Big)\frac{e^{-v^2}}{\pi^{3/2}} \tag{18}$$

the summation being over all background species, including the electrons. It is not difficult to check that $S_i(v)$ automatically preserves the density.

2) The need to include the contribution of the r.h. circularly polarized field component E_- to the QL diffusion coefficient for high-energy ions has been stressed in [8]. In the equations of the previous section this contribution is explicitly included. Comparing solutions of the kinetic equations with and without this term confirms the importance of this term. Here we should also mention, however, that eqn (10) is an approximation. Comparison with the 'exact' expression for $D^p_{\rm ql}$ in terms of the fields evaluated by TORIC (e.g. section 4 of [26]) suggests that eqn (10) is likely to overestimate somewhat the contribution proportional to E_-. Unfortunately, coding the exact $D^p_{\rm ql}$ is a rather complicated task, so that translating this guess into a quantitative statement must be left for future work.

3) Very few Legendre polynomials (up to order 4 or 6) need to be included in the expansion (7) to obtain fully converged profiles of the collisional exchanges between the heated species and the background plasma. For coupling with TORIC, on the other hand, the truncated series (7) itself must be an accurate representation of the QL distribution function up to sufficiently large energies, a much more stringent requirement. The convergence of the Legendre polynomial expansion, therefore, deserves some discussion.

The key for the success of the Legendre expansion is the identity (13). As mentioned

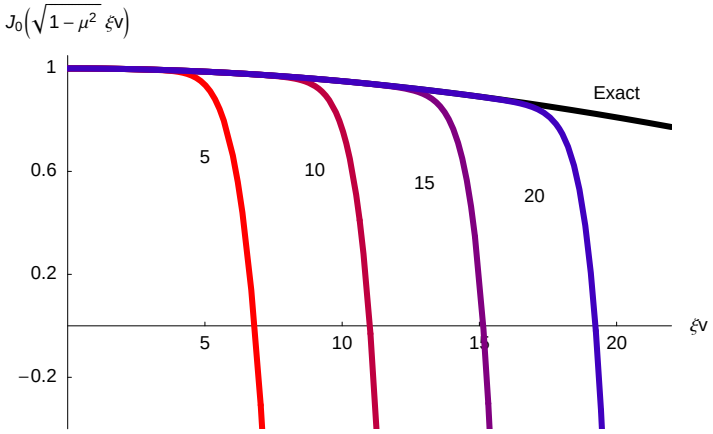

Figure 1. Example of convergence of the Bessel function identity (13) for nearly parallel velocity, $\mu = 0.999$. The envelope is the exact Bessel function on the l.h. side vs $\xi_\perp v$; from left to right the truncated expansion with 5, 10, 15, and 20 Legendre polynomials.

in [7], the rh side of this equation reduces to its first term when $\mu = 0$, and, therefore, the series converges very rapidly for nearly perpendicular velocities, and as long as $v_\parallel \lesssim v_\perp$. More and more terms are needed, on the other hand, to reach convergence as μ approaches unity ($v_\parallel \gg v_\perp$). To give an idea of this behaviour, in figure (1) the exact l.h. side is plotted in the typical range of the argument, together with the series truncated at 5, 10, 15, and 20 terms, for $\mu = 0.999$. The series (7) representing the solution of the kinetic equation behaves similarly, except that the number of terms required for convergence is larger, and, not surprisingly, increases with increasing D_0, i.e. when the hf power absorbed per particle increases. For typical values of the parameters in IC heating experiments, the number of terms required remains nevertheless acceptable in a quite large velocity domain.

It is actually not possible to achieve convergence in the whole velocity space. Above a certain energy the oscillatory behaviour of the Legendre polynomials finally takes over, and the truncated series (7) becomes meaningless in a domain around the $v_\parallel$-axis. While the boundary of the domain where this occurs can in principle always be pushed to higher energies by increasing the number of terms kept, in practice problems of numerical accuracy put an upper limit to the order of the Legendre polynomials which can be included ($N \lesssim 60$ working in double precision). Thus SSFPQL cannot be used to follow the most energetic ions produced in the experiments. It is important to realize, however, that the limiting factor in this respect is not so much the failure of the Legendre expansion at large energies, but, rather, the breakdown of the bounce averaging approximation leading to eqns (9)–(11). Indeed, most of the ions which reach energies exceeding the capability of SSFPQL are on trapped orbits making radial excursions so large that any 'bounce averaged' model is in principle inadequate, even with the corrections for finite banana width discussed in the next section.

Fast ions produced by ICR heating are very interesting [14]: they can relatively

easily be 'seen' by appropriate diagnostics, influence the low frequency stability of the plasma, can be exploited to investigate the behaviour of fusion α-particles in the future reactor, and so on. As mentioned in the introduction, sophisticated Monte Carlo and 'orbit averaging' techniques have been developed to understand their behaviour. The failure of SSFPQL to describe the most energetic of these ions, on the other hand, does in no way interfere with its usefulness for self-consistent simulations of wave propagation and absorption. The reason is that, as is well known and as will be recalled in section 5, the coefficients of the wave equations depend on integral functionals of the distribution functions, rather than on the functions themselves. Although these integrals (particularly those which determine absorption) are far from being insensitive to the presence of suprathermal populations, they clearly are heavily weighted towards the region of velocity space around and up to several times the thermal energy. SSFPQL is reasonably accurate in a range in which F_i decreases by 6 to 12 orders of magnitudes (depending on the collisionality and the hf power available per ion). The error introduced by not accounting for the exponentially few ions beyond this range is small, and completely negligible compared, for example, with the error implicit in using the approximation (10) for the QL diffusion coefficient.

These considerations indicate that in view of building a simple yet accurate model, different approximations are justified in the evaluation of the coefficients of the wave equations and in the solution of the kinetic equation. As a consequence, complete consistency between TORIC and SSFPQL cannot be expected. The renormalization of the coefficient D_0 of the QLO is, therefore, required to achieve convergence of the iterations between the two codes.

4. Accounting for toroidal effects in SSFPQL

1) Equation (10) neglects the toroidal modulation of the parallel velocity in the toroidal magnetic field. In reality, ions transit through resonance only as long as their pitch angle satisfies

$$\mu_{\rm eq}^2 = \frac{v_{\parallel \rm eq}^2}{v^2} \geq \mu_{\rm cr}^2 = 1 - \frac{B_{\rm eq}}{B_{\rm res}} \tag{19}$$

where subscripts "eq" and "res" refer to values at the points where the magnetic surface under consideration crosses the outer equatorial plane and the IC resonance, respectively, and $\mu_{\rm cr}$ denotes the velocity pitch angle at the equatorial plane for which reflection occurs at resonance. Taking into account trapping introduces in the QL diffusion coefficient an additional factor $\mathcal{W}(\psi, v, \mu - \mu_{\rm cr})$ peaked around $\mu_{\rm cr}$. The full expression for $\mathcal{W}$ in terms of the Airy function [27, 28] is rather complicated. For a proof-of-principle that toroidal trapping could be taken into account in SSFPQL, we have used the very rough approximation

$$\mathcal{W} = \mathcal{W}(\mu - \mu_{\rm cr}) = \frac{1}{1 + e^{-\alpha(\mu - \mu_{\rm cr})}} \tag{20}$$

where α simulates the exponential decay of the squared Airy function for ions reflecting before reaching the IC resonance. This allows to capture with a modest numerical

effort (cfr. the last paragraph of Appendix A) the main features of toroidal trapping, in particular the 'ears' in the contour plots of F_i due to the accumulations of ions barely missing the IC resonance (see later, e.g. Fig (11)).

Roughly speaking, eqn (20) is equivalent to neglect the change of the parallel velocity while an ion transits through resonance, an approximation which is manifestly wrong for those ions which are reflected just there, but is consistent with the approximation (10) of the QLDC. For the purpose of coupling SSFPQL with the wave solver, moreover, the consequences of the inaccurate treatment of the transition between resonant and non-resonant ions can again be expected to be reduced by the integral nature of the coefficients of the wave equations. Nevertheless, we have not considered it worth-while performing a full iteration of this rough model of toroidal trapping with the solution of the wave equations, for the following reason. Using eqn (20) (or, for this matter, a more accurate expression for $\mathcal{W}$) gives the distribution function $F_i(v, \mu, \psi, 0)$ at the outer equatorial plane $\vartheta = 0$. To build the coefficients of the wave equations (cfr. the next section), F_i should be remapped to each poloidal position taking into account energy and magnetic moment conservation. The details of the distribution function, on the other hand, influence propagation and absorption only in a relatively narrow region around the position where magnetic surfaces cross the IC resonance. The deformation of F_i due to the toroidal modulation of $v_\parallel$ becomes much smaller when remapped to this position: in particular, the excess trapped ions reflecting before resonance do not contribute, by definition, to the distribution function at the resonance itself. As long as the detailed dynamics of ions reflecting close to resonance is not taken into account, therefore, implementing the rather lengthy and cumbersome remapping procedure does not bring any significant improvement to the SSFPQL model.

2) An even more important limitation of eqn (10) is the assumption that ions are tied to a magnetic surface. For trapped ions, this not entirely true already in the upper range of the energies which most influence wave propagation and absorption. The radial excursions of these ions have two consequences [9]: they broaden the power absorption profiles, and expose the ions to regions of higher collisionality during a non negligible fraction of their orbits.

As long as the width of the banana orbits does not exceed a fraction of the typical gradient length of density and temperature, these effects can be taken into account by recalling that the distribution function is not a function of the radial coordinate ψ, but of the third adiabatic invariant (closely related to the toroidal angular momentum) of the particles [29]

$$\bar{\psi}_{Pg} = \psi_{Pg} - \frac{mc}{Ze}\left[Rv_\parallel \cos\Theta - \omega_B \oint R\cos\Theta\, ds\right] \tag{21}$$

Here $\tan\Theta = B_{\rm pol}/B_{\rm tor}$, ψ_{Pg} is the poloidal flux at the position of the guiding center, $\omega_B = (\oint ds/v_\parallel)^{-1}$ is the transit (or bounce) frequency, and ds is the element of the magnetic field line along which the guiding center would be moving in the absence of perpendicular drift. The integral in eqn (21) vanishes for trapped particles, while for

passing particles the two terms in the brackets very nearly cancel each other. We can therefore approximate

$$\bar{\psi}_{P\,g} \simeq \psi_P + \frac{(\vec{b} \times \vec{\nabla}\psi_P) \cdot \vec{v}_\perp}{\Omega_{ci}} - \frac{mc}{Ze}\, H_{\rm tp}\, R v_\parallel \cos\Theta \tag{22}$$

where ψ_P is the poloidal flux at the radial position of the ion, and we have introduced the Heaviside function $H_{\rm tp}$ which is unity for trapped particles and zero for passing ones. This approximation amounts to neglect the excursions of the guiding center of a passing particle from its average radial position, and breaks down only for a small population of particles near the boundary between passing and trapped. If $\psi = r/a$ is used as radial coordinate instead of ψ_P, we will have, neglecting the classical diamagnetic term compared to the neoclassical one,

$$\bar{\psi}_g \simeq \psi - H_{\rm tp}\, \frac{K_B v_\parallel}{\Omega_{ci}} \qquad\qquad K_B = \frac{BR\cos\Theta}{\mathcal{F}_P(\psi)} \tag{23}$$

with B the local confining magnetic field and $\mathcal{F}_P(\psi) = d\psi_P/d\psi \simeq 2\pi^2(ab/q)\,\psi$, where a and b are the horizontal and vertical radius of the plasma and q the safety factor. Assuming that most trapped particles nevertheless explore a relatively small fraction of the plasma radius, we can 'correct' the quasilinear distribution function for the finite width of the trapped ion orbits by writing, to lowest significant order in the inverse aspect ratio,

$$F_i(v,\mu,\psi) = \sum_n F_n^i(v,\psi)\, P_n(\mu) + \frac{K_B\, v}{\Omega_{ci}}\, \frac{\partial F_0^i(v,\psi)}{\partial\psi}\, \frac{\mu_H^3}{3}\, \mu \tag{24}$$

where

$$\mu_H \simeq \left(\frac{a}{2R_0}\right)^{1/2} \psi^{1/2} \tag{25}$$

Note that once the expression for K_B is inserted in eqn (24), the added term is of order $(r/R)^{1/2}\,\rho_i/a$, except for the fact that $\partial F_0^i/\partial\psi$ must vanish on the magnetic axis. As pointed out e.g. in [30], this correction represents a 'hf-induced' momentum transfer to the ions, akin to the bootstrap current, which exists even if the toroidal power spectrum of the waves is symmetric.

Although eqn (24) was derived to describe broadening of the distribution function by the finite radial excursions of trapped particles, used in the iterative scheme of interactions between TORIC and SSFPQL it also allows to correct for the resulting changes in collisionality. Indeed, at the next iteration of SSFPQL, to the accuracy of the Taylor expansion the collisionality of the particles giving rise to the second term in eqn (25) will be evaluated at the corrected position. It turns out, however, that under realistic conditions this correction has a very small influence on wave propagation and absorption, since it becomes important only at energies so large that are reached by an exponentially small number of ions. This is a fortunate circumstance, because soon above such energies the Taylor expansion (25) (and surface averaging itself) becomes rapidly questionable, and more sophisticated techniques must be used.

5. Ion-Cyclotron frequency range wave equations in non-Maxwellian plasmas.

The coefficients of the wave equations solved by TORIC are closely related to the elements of the dielectric tensor of hot plasmas, whose expressions for arbitrary distribution functions can be found e.g. in Section 14 of [31]. In the IC range of frequencies it is sufficient to write these coefficients in the reduced Finite Larmor Radius (FLR) approximation (the only exception occurs for the description of ion Bernstein waves, to be briefly discussed below). In reference [32], moreover, it has been shown that in the IC range of frequencies the deviations of the electron distribution function from Maxwellian have an insignificant influence on the coefficients of the wave equations. This is due to the large e/m ratio of the electrons, together with the fact that, in contrast with the lower hybrid case, in the IC range electron absorption occurs mostly in the thermal domain. Taking this into account, and using the notations of [2], the coefficients affected by deviations from local thermal equilibrium are

$$\begin{aligned}
\hat{L} \quad &= 1 + \frac{\omega_{pe}^2}{\Omega_{ce}^2} - \sum_i \frac{\omega_{pi}^2}{\omega^2}\,\pi \int_0^\infty w\,dw\Big(- x_0 \int_{-\infty}^{\infty} \frac{\mathcal{F}_\perp^i(w,u)}{u - x_1}\,du\Big) \\
\hat{\lambda}_i^{(2)} &= \frac{1}{2}\frac{\omega_{pe}^2}{\Omega_{ce}^2}\frac{v_{the}^2}{c^2} + \sum_i \frac{\omega_{pi}^2}{\Omega_{ci}^2}\,\frac{v_{thi}^2}{c^2}\,\frac{\pi}{4} \int_0^\infty w^3\,dw\Big(- x_0 \int_{-\infty}^{\infty} \frac{\mathcal{F}_\perp^i(w,u)}{u - x_2}\,du\Big)
\end{aligned} \tag{26}$$

where

$$\mathcal{F}_\perp^\alpha(u,w) = -w\Big(\frac{\partial F_\alpha}{\partial w} + \frac{k_\parallel v_{th\alpha}}{\omega}\,\Theta_v F_\alpha\Big) \tag{27}$$

Here $u = v_\parallel/v_{th\alpha}$, $w = v_\perp/v_{th\alpha}$ (here $v_{th\alpha}$ is the thermal speed of species α in the background plasma), and

$$\Theta_v F = w\frac{\partial F}{\partial u} - u\frac{\partial F}{\partial w} \tag{28}$$

is the derivative operator over the velocity pitch angle, which vanishes for isotropic distributions. Finally

$$x_p = \frac{\omega - p\Omega_{c\alpha}}{k_\parallel^{mn} v_{th\alpha}} \qquad\qquad k_\parallel^{mn} = \frac{m + qn}{R h_s}, \qquad h_s = 1 + \frac{N_\vartheta^2}{q^2 R^2} \tag{29}$$

($N_\vartheta = \sqrt{g_{\vartheta\vartheta}}$ is the elements of the metrics of toroidal coordinates which reduces to the minor radius r in the limit of circular magnetic surfaces). We stress that $k_\parallel$ has to be separately evaluated for each poloidal Fourier component of the wave fields.

A further important simplification follows from the fact that for ions the inequality $k_\parallel v_{thi}/\omega \ll 1$ is always satisfied by a large margin in the IC range. Neglecting, therefore, the second term in eqn (27), it is convenient to rewrite eqns (26), after integration by

parts and for a real frequency ω, as

$$\begin{aligned}\hat{L} \quad &= 1 + \frac{\omega_{pe}^2}{\Omega_{ce}^2} - \sum_i \frac{\omega_{pi}^2}{\omega^2}\Big[- \bar{x}_0 \,\mathrm{P}\int_{-\infty}^{\infty} \frac{F_i^{(0)}(u)}{u - \bar{x}_1}\, du - i\pi\, \bar{x}_0\, F_i^{(0)}(x_1)\Big] \\ \hat{\lambda}^{(2)} &= \frac{1}{2}\frac{\omega_{pe}^2}{\Omega_{ce}^2}\frac{v_{the}^2}{c^2} + \frac{1}{2}\sum_i \frac{\omega_{pi}^2}{\Omega_{ci}^2}\frac{v_{thi}^2}{c^2}\Big[- \bar{x}_0 \,\mathrm{P}\int_{-\infty}^{\infty} \frac{F_i^{(2)}(u)}{u - \bar{x}_2}\, du - i\pi\, \bar{x}_0\, F_i^{(2)}(x_2)\Big]\end{aligned} \tag{30}$$

where we have introduced the moments of the distribution function with respect to the perpendicular velocity

$$F^{(2s)}(u) = 2\pi \int_0^{\infty} F_i(u, w)\, w^{2s+1}\, dw \tag{31}$$

($s = 0$, 1; in the following, these moments will be called for brevity "reduced distribution functions"; the functions in the brackets of eqns (30) are known as Generalized Plasma Dispersion Function, GPDF).

To take into account large Larmor radius effects, the definition of $F^{(2)}$ in the terms describing IB waves should be modified as follows

$$F^{(2)}(u) = \frac{16\pi}{\xi_\perp^2} \int_0^{\infty} F_i(u, w)\, J_2^2(\xi_\perp w)\, w\, dw \tag{32}$$

with $\xi_\perp = k_\perp v_{thi}/\Omega_{ci}$, $k_\perp$ being the local perpendicular wavevector of the IB wave. This would be numerically rather demanding; in practice, however, the approximation (30) is sufficient throughout. In the critical regions where mode conversion between Fast and IB waves occurs eqns (30)-(31) are still quantitatively justified. Far from mode conversion, on the other hand, where for IB waves $k_\perp v_{thi}/\Omega_{ci} \gtrsim 1$, parallel dispersion is negligible, so that the local dispersion relation of IB waves is influenced mainly by the perpendicular pressure, rather than by the details of the distribution function. Thus eqns (30)-(31) give a fair approximation over the whole range where IB waves are propagating.

6. Numerical evaluation of the plasma response

According to eqns (30)-(31), the task of evaluating the coefficients of the IC wave equations for non-Maxwellian plasmas splits into two steps: the evaluation of the moments (31), and that of the singular integrals (30). To justify our approach for the solution of these tasks, let us first make a few comments on the results of the previous section.

1) The moments (31) can be evaluated with a standard integration scheme. Since $F^i(v)$ is provided by the kinetic solver in a spherical region, the accuracy by which these integrals can be evaluated inevitably degrades somewhat in the upper velocity range. This can be tolerated, as long as the result is accurate in the domain important for propagation and absorption of the waves.

2) The evaluation of the singular integrals of the type

$$\mathcal{Z}(x_p) = \int_{-\infty}^{+\infty} \frac{F(u)}{u - x_p}\, du \qquad\qquad \mathrm{Im}(\omega) \to 0+ \tag{33}$$

where $F(u)$ stays for any of the moments defined in eqn (31), is more difficult: the imaginary part requires only the knowledge of the moments $F_i^{(2s)}(u)$, but an ad-hoc algorithm must be developed for the real part, which is a principal part integral in the sense of Cauchy. These singular integrals are needed by the wave solver not only for a large number of values of the argument x_p (we recall that each Fourier component of the field has its own phase velocity, which varies from point to point on each magnetic surface), but also on a dense mesh of the radial coordinate ψ. In practice, the number of evaluations needed can easily exceed 10^7 to 10^8. Clearly, an efficient algorithm is needed to keep the numerical burden within acceptable limits.

3) The radial smoothness of the functions $\mathcal{Z}(x)$ is as important as the accuracy, since any irregularity of the coefficients of the wave equations is interpreted as a scattering center for the waves. ion Bernstein and shear waves, when propagative, are particularly sensitive to this effect.

An algorithm which satisfies all the conditions imposed by these considerations has been developed by expanding an idea of Valeo [22]. The real part of the integral (33) can be rewritten

$$\begin{aligned} G(x) &= \mathrm{P}\int_{-\infty}^{+\infty} \frac{F(u)}{u-x}\,du = \lim_{\epsilon\to 0}\Big(\int_{-\infty}^{x-\epsilon} + \int_{x+\epsilon}^{+\infty}\Big)\frac{F(u)}{u-x}\,dx \\ &= \lim_{\epsilon\to 0}\int_0^{\infty}\left[\frac{F(y+x+\epsilon)}{y+\epsilon} - \frac{F(-y+(x-\epsilon))}{y-\epsilon}\right]dy = \int_0^{\infty}\frac{F(x+y)-F(x-y)}{y}\,dy \end{aligned} \tag{34}$$

$G(x)$ is known as the Hilbert transform of $F(x)$. We note that under the assumption that $F(u)$ is continuous and continuously differentiable the last form is free from singularities, since then

$$\lim_{y\to 0}\frac{F(u+y)-F(u-y)}{y} = 2F'(u) \tag{35}$$

Let us now assume that the kinetic solver has calculated $F(u_j) = f_j^{(0)}$ on the current magnetic surface at the points of an equidistant parallel velocity mesh. It is then expedient to evaluate $G(x)$ at the same points $x = u_j$, and then interpolate, e.g. with cubic splines, according to the needs of the wave solver. On the jth interval of the u mesh we can approximate $F(u)$ by a linear function

$$F(u) \simeq f_j^{(0)} + f_j^{(1)}(u-u_j) \qquad\qquad u_j \le u_{j+1} = u_j + \Delta \tag{36}$$

where, to guarantee continuity,

$$f_j^{(1)} = \frac{f_{j+1}^{(0)} - f_j^{(0)}}{\Delta} \tag{37}$$

We can then write

$$F(u) \simeq \sum_j \Big[f_j^{(0)} + f_j^{(1)}(u-u_j)\Big]\theta_j(u) \qquad\qquad \theta_j(u) = \begin{cases} 1 & \text{if } u_j \le u \le u_{j+1} \\ \\ 0 & \text{elsewhere} \end{cases} \tag{38}$$

Inserting this into the definition of G, and denoting with a prime a summation excluding the two intervals adjacent to the point $x_j = u_j$, we get

$$G(u_j) \simeq \sum_k{}' \left\{ \left[f_k^{(0)} + f_k^{(1)}(u_j - u_k) \right] \log \frac{u_k - u_j + \Delta}{u_k - u_j} + f_k^{(1)}\,\Delta \right\} + f_{j+1}^{(0)} - f_{j-1}^{(0)} \tag{39}$$

To evaluate the last two terms we have put the contribution of the two intervals adjacent to u_j in the last form of eqn (34), and we have approximate the derivative of F by a centered difference. Note that the weights in this summation depend only on the difference $u_j - u_k$, and are, therefore, a one-dimensional array which, moreover, needs to be evaluated only once, since the values of its elements are manifestly independent from the mesh step. Eliminating $f_k^{(1)}$, we can rewrite (39) as

$$\begin{aligned} \mathcal{Z}(u_j) \simeq f_{j+1}^{(0)} - f_{j-1}^{(0)} + \sum_{k=1}^{\infty} \Big\{ & C_k \Big(f_{j+k}^{(0)} - f_{j-k}^{(0)} \Big) \\ & - D_k \Big[\Big(f_{j+(k+1)}^{(0)} - f_{j+k}^{(0)} \Big) - \Big(f_{j-(k+1)}^{(0)} - f_{j-k}^{(0)} \Big) \Big] \Big\} \end{aligned} \tag{40}$$

with

$$C_k = \log \frac{k+1}{k} \qquad\qquad D_k = k \log \frac{k+1}{k} - 1 \tag{41}$$

The coefficients have the symmetries $C_{-(j+1)} = -C_j$, $D_{-(j+1)} = -D_j$, and tend (slowly) to zero for large j.

The above procedure only enables to evaluate the generalized $\mathcal{Z}$ functions inside the velocity interval in which SSFPQL solves the kinetic equations, and the moments (31) can be evaluated with sufficient accuracy, typically $|u| \leq 7$ to 8. Outside this range the number of resonant ions is very small, the imaginary part of $\mathcal{Z}$ is negligible, and the real part can be evaluated using the asymptotic development

$$\mathcal{Z}(x) \simeq -\frac{1}{x} \int_{-\infty}^{+\infty} F(u) \left(1 + \frac{u}{x} + \frac{u^2}{x^2} + \dots \right) du \tag{42}$$

With some attention to the way the summations in eqn (40) and (42) are truncated, the evaluation of the Hilbert transform with this algorithm is both fast and accurate: a relative error $\lesssim 10^{-6}$ is easily obtained by applying this technique to the case of a Maxwellian distribution, in which independent and very accurate algorithms for the evaluation of $\mathcal{Z}$ are available.

For the efficiency of the whole approach, care is also to be devoted to the interface between the quasilinear kinetic solver SSFPQL and the wave solver TORIC. It would not be reasonable, to begin with, to solve the kinetic equations on all the magnetic surfaces required by the wave solver. Instead, we let the kinetic solver evaluate $F(u_j)$ on a radial mesh sufficient to ensure a smooth radial variation, leaving to the wave solver the task of interpolating in the radial variable ψ. It is also easily seen, on the other hand, that to interpolate the functions $F(u_j)$ themselves would be cumbersome, and would pose serious accuracy and smoothness problems. It is far more convenient to determine on each magnetic surfaces of the SSFPQL mesh a best fit to the moments (31)

of the solution of the kinetic equation and to the corresponding Hilbert transforms using an appropriate set of basis functions with a moderate number of parameters. We then let the wave solver interpolate radially these parameter to reconstruct functions and integrals as required for the evaluation of the stiffness matrix of the wave equations. With due care to the choice of the interpolating functions, this approach can be made both robust and efficient. It also keeps within very moderate bounds the amount of information to be transmitted from the kinetic to the wave solver.

Concretely, the w^{2s}-moments of distribution function are fitted by exponentials of the form

$$F^{(2s)}(u) \simeq e^{-[K_s + a_s u^2/\Lambda_n^s(u)]} \tag{43}$$

where K_s is a normalization constant, and $\Lambda_n^s(u)$ a polynomial of order n in u. The Hilbert transform are interpolated by rational functions,

$$G^{(2s)}(u) \simeq \frac{u\, P_n^s(u)}{1 + u^2\, Q_n^s(u)} \tag{44}$$

where P_n^s and Q_n^s are polynomials of order n. In this case, a special initialization of the fitting procedure has been implemented to avoid situations in which numerator and denominator would change sign almost simultaneously inside the interval where the fitting is to be used. The coefficients of the fitting polynomials are then determined using standard routines adapted from [33]. In both cases polynomials of 4th to 6th order give excellent fits (typically, with relative error $\lesssim 10^{-4}$ in the entire range $-8 \lesssim u \lesssim +8$), while the accuracy improves only slowly by using polynomials of higher order.

The numerical implementation is greatly simplified by letting SSFPQL evaluate the moments (31) of the quasilinear distribution functions, their Hilbert transforms with the algorithm (39), and the coefficients of the fitting polynomials in eqns (43) and (44), on each magnetic surface as soon as the kinetic equation on that surface has been solved. The coefficients of the fitting polynomials evaluated at the points of the radial mesh of SSFPQL (typically 100 magnetic surfaces) are read by TORIC, and interpolated with cubic splines on the much finer radial mesh required to solve Maxwell equations. The whole procedure demands a few seconds, compared with several minutes for the solution of the Fokker-Planck equations, and a similar or longer time for the solution of Maxwell equations. Finally, on each magnetic surface of its own radial mesh, and for each poloidal Fourier mode of the wave field, TORIC evaluates the generalized Z functions (33) at the points of the poloidal mesh using the fitting functions (43)-(44). This last step replaces the evaluation of the Plasma Dispersion Function in the Maxwellian case.

7. An example

As an example of application of the TORIC-SSFPQL package, we have analyzed the same minority heating scenario as in [1] (6% H in a D plasma; central electron density 6.53 10^{19} m^{-3}, central temperatures $T_e = 4.35$ keV, $T_i = 4.33$ keV) in ASDEX Upgrade. Figure 2 shows Re(E_+) and Re(E_-) in the poloidal cross-section for the

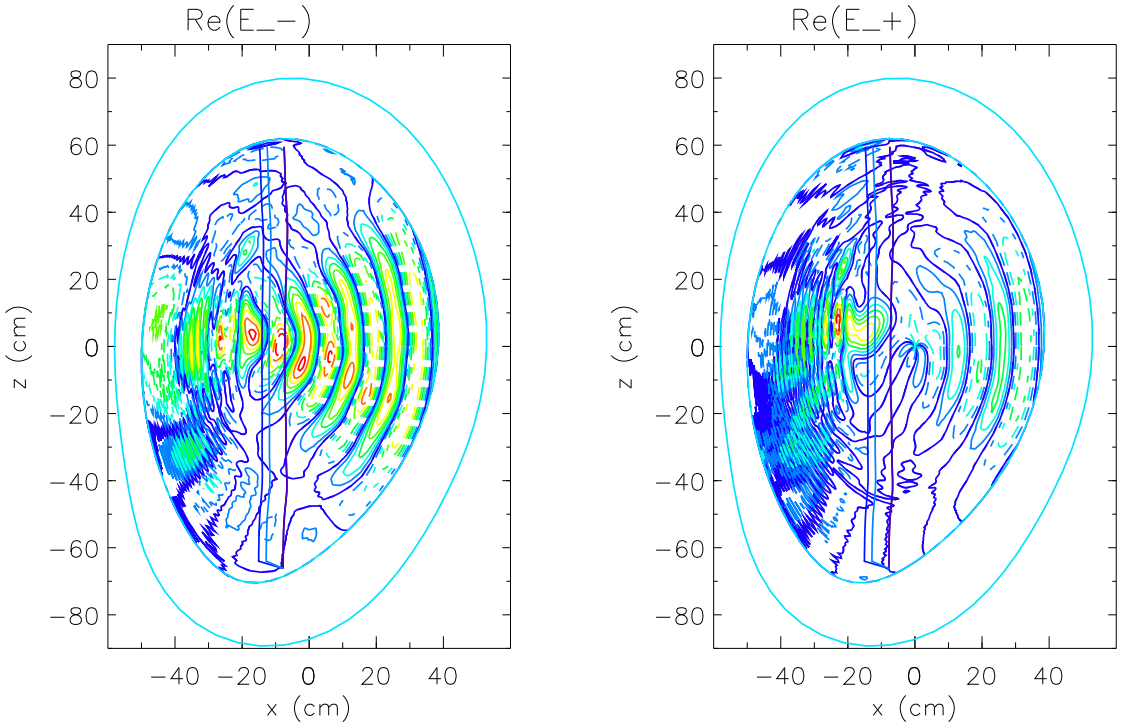

Figure 2. Re(E_+) and Re(E_-) in the poloidal cross-section, Maxwellian plasma

average toroidal mode $n_\varphi = 12$, and the position of the main singularities. With a central magnetic field of 1.97 Tesla, the applied frequency of 30.5 MHz puts the cyclotron resonances 7.3 cm to the high field side of the magnetic axis, while the ion-ion cutoff and resonances are further inside, at -11.9 cm and -14.1 cm, respectively. From plots of these fields along the equatorial plane, one can deduce a high single transit absorption, since there is almost no standing wave between the antenna and the ion-ion cutoff; further, as expected, $|E_+| \lesssim |E_-|/3$, with a marked minimum near the IC resonance, except to the high-field side of the ion-ion resonance, where the field pattern is dominated by linearly polarized Ion Bernstein waves. Note that the IB waves transport very little power, just about 1.1% of the total; the associate fields are nevertheless large because of the very slow group velocity of these nearly electrostatic waves. Figure 3 reports the power deposition profiles in the Maxwellian plasma, normalized to 1 MW total coupled power. Integrated over the plasma, 65.54% of the power is absorbed by the minority Hydrogen, 18.33% by the Deuterium by first harmonic heating, and 16.13% by the electrons, including 1.1% from the IB wave.

In the first place, as a check of the accuracy of the entire procedure, we have run SSFPQL assuming zero hf power. In this limit, SSFPQL evaluates the coefficients for the interpolation of the distribution functions and of the Plasma Dispersion Function in the Maxwellian limit. These data have then been used to run TORIC again. The power deposition profiles and the pattern of the fields obtained were identical to those of the previous run, the relative differences never exceeding 10^{-3} over the whole cross-

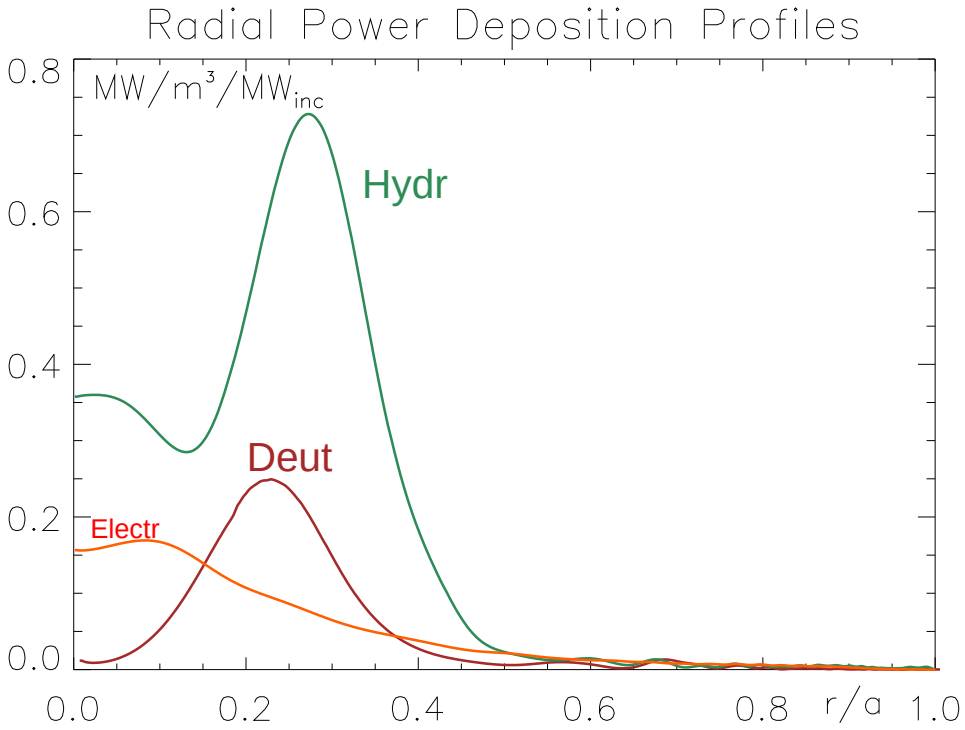

Figure 3. Power deposition profiles in the Maxwellian plasma.

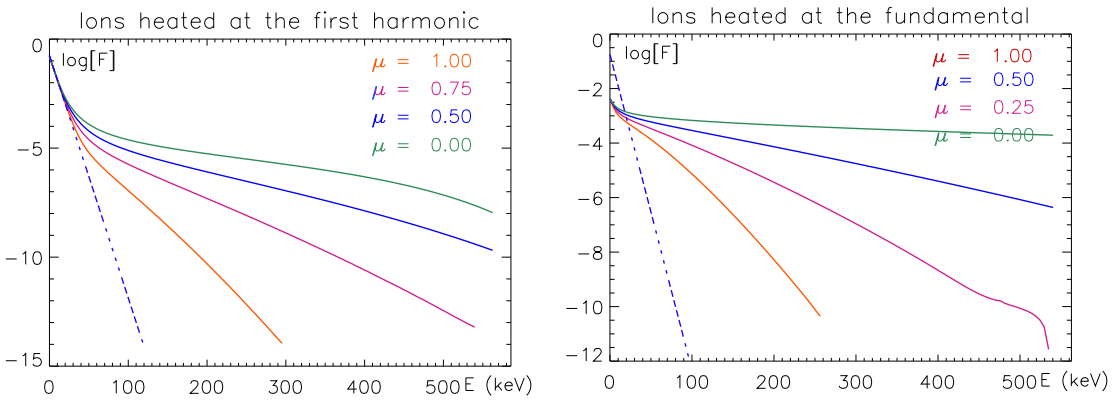

Figure 4. Quasilinear distribution functions: semilog plots vs energy at 5 values of the pitch angle, at the position of peak absorption: a) harmonic heated Deuterium; b) Hydrogen heated at the fundamental.

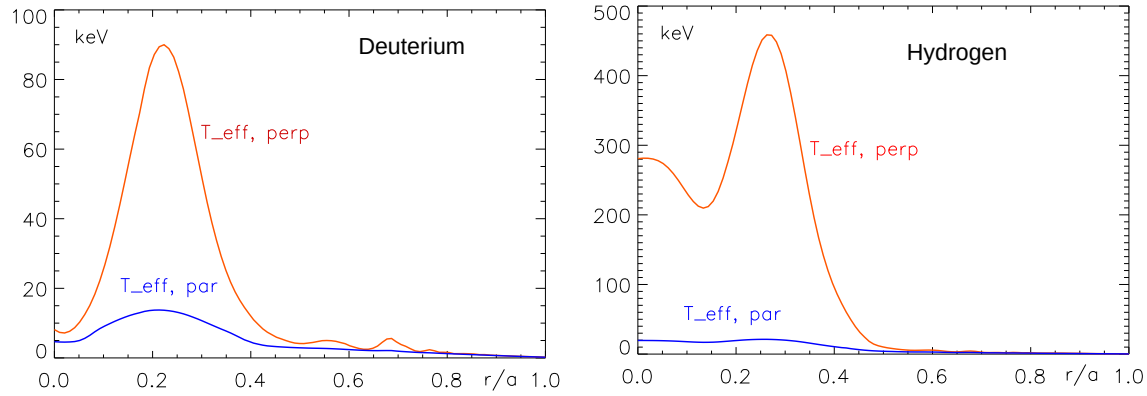

Figure 5. Parallel and perpendicular tail temperatures vs radius: a) harmonic heated Deuterium; b) Hydrogen heated at the fundamental.

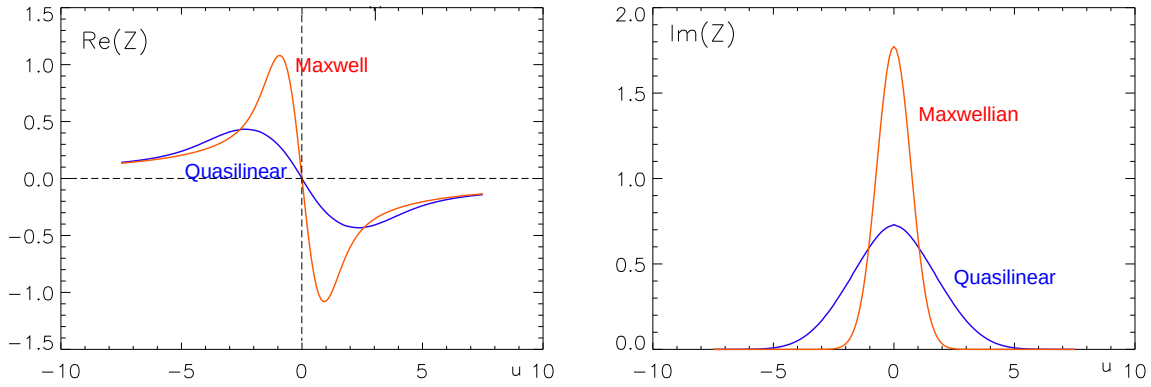

Figure 6. $\mathrm{Re}(\mathcal{Z}(x_1))$ and $\mathrm{Im}(\mathcal{Z}(x_1))$ for the Hydrogen at the point of peak absorption.

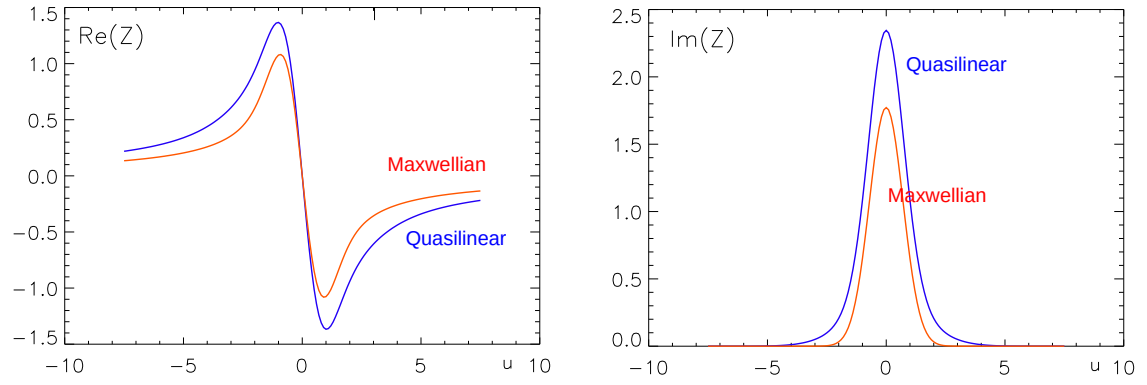

Figure 7. $\mathrm{Re}(\mathcal{Z}(x_2))$ and $\mathrm{Im}(\mathcal{Z}(x_2))$ for the Deuterium at the point of peak absorption.

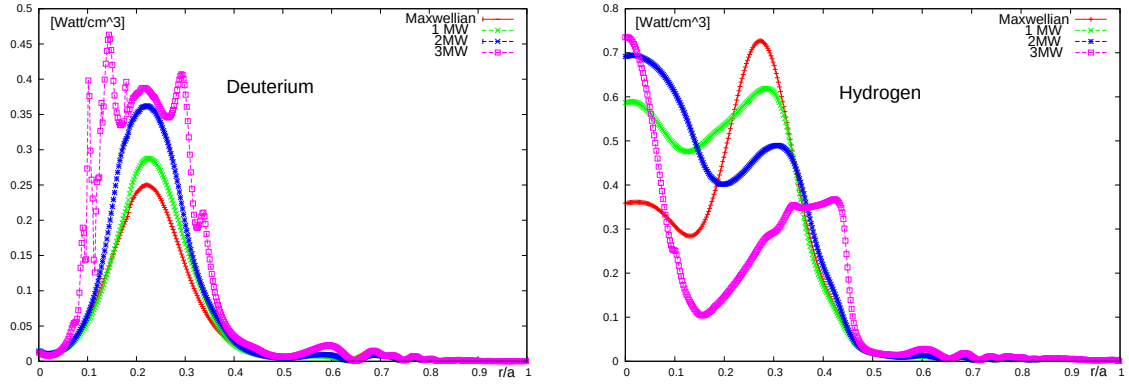

Figure 8. Power deposition profiles for Hydrogen and Deuterium (normalized per MW coupled power) at different total power levels.

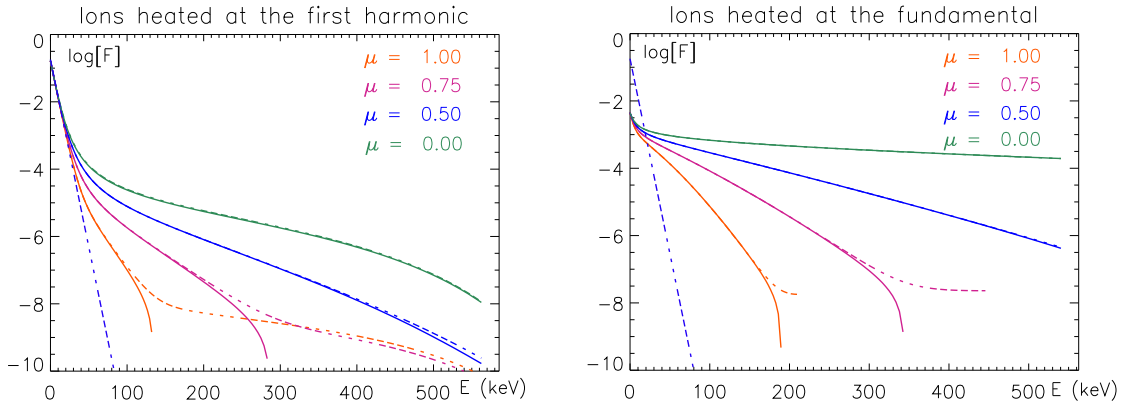

Figure 9. Same as fig. 4, but including finite orbits effects. Full lines $v_{\|} > 0$, dashed lines $v_{\|} < 0$.

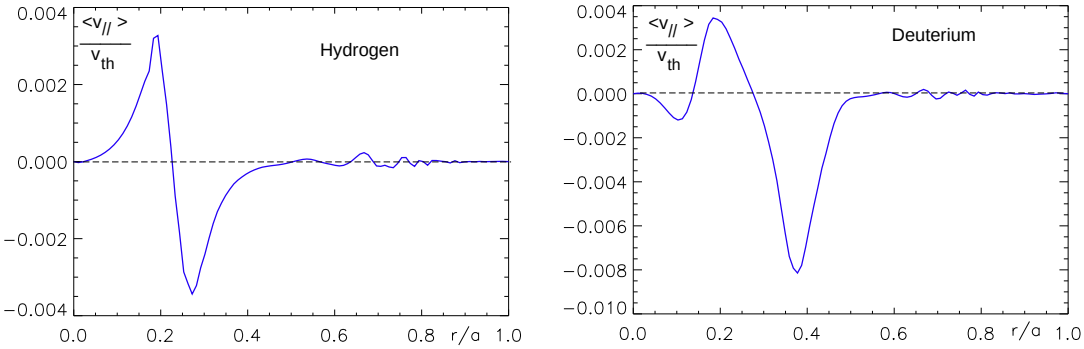

Figure 10. Radial profile of $\langle v_{\|} \rangle / v_{th}$ taking into account finite orbits corrections.

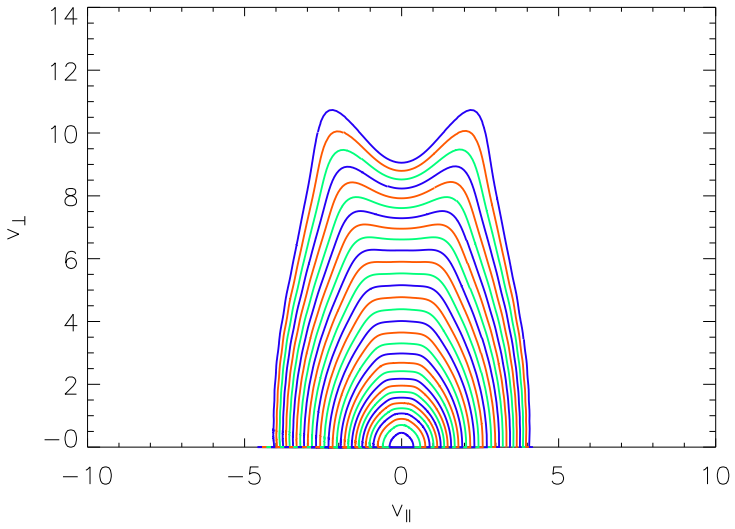

Figure 11. Contour plot of the minority distribution function at the point of peak absorption taking into account toroidal trapping (total hf power 2 MW).

section. The run of TORIC using the data from SSFPQL in the way described above was actually 20% faster than the initial run assuming from the beginning Maxwellian distribution functions, a good confirmation of the efficiency of our approach.

Before considering the iteration between TORIC and SSFPQL, it is appropriate to present a few results from SSFPQL itself, which illustrate and complement the discussion of sections 3 and 4. The total coupled power was assumed 3 MW, about the maximum value reached in the experiments (the power deposition profiles, therefore, are 3 times higher than those of Figure 3). Figure 4 shows semilogarithmic plots of the quasilinear distribution functions versus energy for a few values of the velocity pitch-angle, at the radial position corresponding to the maximum of power absorption. The tails are quite energetic (in the region of strong absorption the partial pressure of the heated minority becomes comparable to the pressure of the background plasma) and very anisotropic. The effective perpendicular and parallel temperature (estimated from the logarithmic energy derivatives) are shown versus radius in Figure 5.

It must be mentioned that the effective temperatures ($T_{\rm eff}$) predicted by SSFPQL are considerably higher than those observed experimentally, which for the minority species are in the range of 80 to 150 keV. Several causes might contribute to this discrepancy. 1) The plasma of ASDEX Upgrade in not entirely transparent to charge-exchange neutrals, so that the distributions measured might reflect the situation somewhat to the outside of the peak of power absorption. 2) The power reaching the plasma core in the experiments might be somewhat lower than the power radiated by the antenna, due to parasitic effects in the plasma periphery. 3) The SSFPQL model of the quasilinear diffusion coefficient, eqn (3), is likely to overestimates the role of E_- (even if the term proportional to E_- is omitted, however, the discrepancy decreases somewhat,

but does not disappear). 4) In our opinion, however, the most important cause of discrepancy is the absence of a loss term in the SSFPQL model. In the energy range considered here direct losses of ions to the wall are negligible, and losses by rf-induced transport are very small. On the other hand, transport of fast ions due to interactions with the low-frequency turbulence responsible of anomalous transport (which, in turn, could be influenced by the presence of suprathermal populations) is likely to be an important factor in determining the steady-state shape of the quasilinear distributions. A realistic model of how such losses depend on energy and pitch angle is, unfortunately, not available. A few simple heuristic loss models have been proposed, but since they introduce a large degree of arbitrariness in the results, we have preferred not to include them in the code for the moment. One has to be aware, therefore, that the results presented are likely to correspond to rather higher values of the total hf power than assumed here.

For the purpose of coupling SSFPQL with TORIC, of central importance are the generalized Plasma Dispersion Functions (GPDF) $\mathcal{Z}$ defined in eqn (33). Those relevant for the present scenario, namely $\mathcal{Z}(x_1)$ for Hydrogen and $\mathcal{Z}(x_2)$ for Deuterium, are shown in Figures 6 and 7, again at the position of peak power absorption. The quasilinear broadening of $\mathcal{Z}(x_1)$ not only increases the Doppler width of the minority cyclotron damping region, but also reduces the screening of E_+ near resonance. It is important to note, therefore, that this broadening corresponds to an effective temperature somewhat larger than the effective parallel temperature of the Hydrogen tail, but much smaller than its effective perpendicular temperature. Since the absorbed power per Deuterium ion is quite modest in this scenario, the GPDF of Deuterium is much less affected by the heating. There is, however, an important difference between fundamental and first harmonic. While $F^{(0)}(u)$ (eqn (31)) is normalized to unity independently of the heating rate, $F^{(2)}(u)$ is normalized to $\langle v^2 \rangle$, so that the area under $\mathrm{Im}(\mathcal{Z}(x_2))$ and the absolute values of $\mathrm{Re}(\mathcal{Z}(x_2))$ increase when the heating rate increases. This is a consequence of the fact that IC harmonic heating is a finite Larmor radius effect.

The consequences of this behaviour can be seen in Figure 8, which shows the evolution of the power deposition profiles of majority and minority as the total coupled power increases. Doppler broadening of the Hydrogen cyclotron resonance is manifest, but competion from Deuterium increasingly indent the Hydrogen absorption profile. The profiles at 1 and 2 MW reach convergence (roughly within one percent accuracy) in two and three iterations, respectively. At 3 MW, on the other hand, full convergence is not reached. The profiles plotted for this case are obtained after four iterations. Although the global power balance does not significantly change between the third and the fourth iteration (the fraction absorbed by D^+ has increased to 35%, entirely at the expense of H^+), the great sensitivity of harmonic heating to the particle energies above a certain level enhances the small unavoidable local irregularities in the damping rate, producing the spikes visible in the upper curve of the Deuterium plots. We stress that this 'instability' is not created by the numerics, which only provides the seeds for the growth of the spikes, but is intrinsic to the physical model. Of course, we expect that

the inclusion of a realistic loss term would largely suppress this behavior, and probably reduce the competition of the majority in favour of fundamental heating of the minority.

Finally, we have investigate the importance of the corrections (25) for the finite radial width of banana orbits. Figure 9 is the same as Figure 4, but taking these corrections into account. The resulting asymmetry between co-moving and counter-moving ions is clearly visible in the upper energy range. The imbalance in the average parallel velocity, although small (well below 1% of the thermal speed), is measurable, and has the typical bipolar radial profile shown in Figure 10. Since the asymmetry affects only a fraction of ions of the order of one in 10^6, however, the effects on the coefficients of the wave equations are too small to be visible on the scale of figures 6 and 7, and have no measurable influence on the results of the iterations between TORIC and SSFPQL.

For completeness, in fig. 11 we show the contour plot of the minority distribution function predicted by SSFPQL at the point of peak absorption when the effect of toroidal trapping on the number of ions transiting through resonance is taken into account according to eqn (20). We recall, however, that this model is only qualitative. As mentioned in section 4, moreover, fig. 11 gives the distribution function at the outer equatorial plane, and not at the position of the cyclotron resonance, where its shape influences absorption.

8. Conclusions

We have implemented a package for the self-consistent evaluation of wave propagation and absorption in the Ion Cyclotron range of frequency, taking into account the quasilinear evolution of the ion distribution functions. To make this package fast and nevertheless accurate we have taken advantage of the fact that the coefficients of the wave equations are integral functionals of the distribution functions, and are most sensitive to deviations from Maxwellians in the domain from just above to several times the thermal energy. Accordingly, our effort has been devoted to ensure that our kinetic solver SSFPQL gives a reliable solution in this range, while accepting that this code is not designed to follow the exponentially few but extremely energetic ions also produced by IC resonances. We have also shown that in the relevant range of energies the radial excursions of trapped ions do not significantly influence the self-consistent power deposition profiles, and that, within our simplified model (eqn (10)) of the QLDC, no significant improvement would result by taking into account the trapping of ions in the toroidal magnetic field. On the other hand, we have identified an important missing element in the self-consistent Maxwell-quasilinear simulations of IC heating experiments, namely the unavailability of an adequate model of the anomalous losses of suprathermal ions. To build such a model would require a much broader experimental data basis (including space resolved absolute flux values) than presently available. On the other hand, trying to obtain these data could shed interesting light also on the loss mechanisms of fast ions and alpha particles in the reactor. The TORIC-SSFPQL

package could be a useful tool for this task. For this purpose, however, the Monte Carlo approach might again be of advantage, since most easily allows to incorporate additional effects, such as neoclassical and magnetic ripple diffusion, or diffusion due to low frequency fluctuations.

It is worth mentioning again that the Legendre polynomials expansion of the distribution functions used by SSFPQL cannot be expected to converge in the whole velocity space. We have made an effort, therefore, to ensure that convergence is reached in a domain sufficiently large, so that ignoring what happens outside it will not appreciably influence the coefficients of the wave equations. This is not always trivial. Although several criteria have been developed, and warnings are issued when failings are detected, the variety of IC heating scenarios is so large that it is difficult to predict what could go wrong in all situations. To avoid erroneous conclusions, it is always recommended to check by visual inspection the results of SSFPQL before accepting them for iteration with TORIC. We hope that this situation will improve, as experience with the use of the code will suggest more refined and generally reliable convergence criteria.

In spite of this limitation, we hope to have made it plausible that SSFPQL is adequate for the purpose of determining the main part of the quasilinear ion distribution functions, and thus for coupling with a wave solver for self-consistent simulations of wave propagation and absorption in the IC range of frequencies.

Acknowledgments.

The code TORIC has benefitted of important contributions from P. T. Bonoli, E. D'Azevedo, D. McCune, F. Meo, and J.C. Wright.

9. Appendix

The integrals over Legendre polynomials required by SSFPQL are listed in eqns (17). Only the integrals in which n and m are either both even or both odd are different from zero. The following integrals, moreover, vanish for all values of p and k:

$$\begin{aligned} &Q^p_{01}(n,0,k) = Q^p_{10}(0,m,k) = 0 \\ &Q^p_{11}(0,0,k) = Q^p_{11}(n,0,k) = Q^p_{11}(0,m,k) = 0 \end{aligned} \tag{A1}$$

We note the symmetries

$$\begin{aligned} Q^p_{00}(n,m,k) = Q^p_{00}(m,n,k) \qquad & Q^p_{11}(n,m,k) = Q^p_{11}(m,n,k) \\ Q^p_{10}(n,m,k) &= Q^p_{01}(m,n,k) \end{aligned} \tag{A2}$$

and, again for all values of p and k,

$$\begin{aligned} Q^p_{01}(n,1,k) = Q^p_{0,0}(n,1,k) \qquad & Q^p_{10}(1,m,k) = Q^p_{0,0}(1,m,k) \\ Q^p_{11}(1,1,k) &= Q^p_{0,0}(1,1,k) \end{aligned} \tag{A3}$$

(the first two are equivalent because of the symmetries).

For our purpose, it is convenient to introduce the auxiliary integrals, which we will call of the first, second, and third kind, respectively ‖:

$$\begin{aligned} X^p(n,m,k) &= \int_{-1}^{+1} P_n(\mu)\,(1-\mu^2)^{1+p}\,\mu^k\,P_m(\mu)\,d\mu \\ Y^p(n,m,k) &= \int_{-1}^{+1} P_n(\mu)\,(1-\mu^2)^{1+p}\,\mu^k\left(\mu\frac{dP_m}{d\mu}\right)d\mu \\ Z^p(n,m,k) &= \int_{-1}^{+1} \left(\mu\frac{dP_n}{d\mu}\right)(1-\mu^2)^{1+p}\,\mu^k\left(\mu\frac{dP_m}{d\mu}\right)d\mu \end{aligned} \tag{A4}$$

so that

$$\begin{aligned} Q^p_{00}(n,m,k) &= X^p(n,m,2k) \\ Q^p_{01}(n,m,k) &= Y^p(n,m,2k) \\ Q^p_{11}(n,m,k) &= Z^p(n,m,2k) \end{aligned} \tag{A5}$$

Recalling

$$P_0(\mu) = 1 \qquad\qquad P_1(\mu) = \mu\frac{dP_1}{d\mu} = \mu \tag{A6}$$

one can express the non-vanishing integrals with $n = m = 0$ and $m = n = 1$ in terms of the integral

$$\mathcal{I}(p,k) = \int_{-1}^{+1}(1-\mu^2)^p\,\mu^{2k}\,d\mu = \frac{\Gamma(1+p)\Gamma(1/2+k)}{\Gamma(3/2+k+p)} = \frac{p!}{\prod_{i=k}^{k+p}(i+1/2)} \tag{A7}$$

All non-zero integrals with higher indexes can be evaluated from these using the recursion relations

$$P_n(\mu) = 2\mu\,P_{n-1} - P_{n-2} - \frac{1}{n}\left[\mu\,P_{n-1} - P_{n-2}\right] \tag{A8}$$

and

$$\frac{dP_n}{d\mu} = \frac{dP_{n-2}}{d\mu} + (2n-1)P_{n-1} \tag{A9}$$

a) The integrals of the first kind satisfy the recursion relations

$$\begin{aligned} X^p(n,m,k) &= 2X^p(n-1,m,k+1) - X^p(n-2,m,k) \\ &\qquad - \frac{1}{n}\Big[X^p(n-1,m,k+1) - X^p(n-2,m,k)\Big] \\ &= 2X^p(n,m-1,k+1) - X^p(n,m-2,k) \\ &\qquad - \frac{1}{m}\Big[X^p(n,m-1,k+1) - X^p(n,m-2,k)\Big] \end{aligned} \tag{A10}$$

‖ All integrals (A4) have to be used, rather than only those listed in eqn (17) if the distribution functions are not assumed to be simmetric in $v_\parallel$

initialized for all k by

$$\begin{aligned} X^p(0,0,2k) &= \mathcal{I}(p+1,k) \\ X^p(1,1,2k) &= \mathcal{I}(p+1,k+1) \\ X^p(0,1,2k+1) &= \mathcal{I}(p+1,k+1) \end{aligned} \tag{A11}$$

b) The integrals of the second kind satisfy the recursion relations

$$\begin{aligned} Y^p(n,m,k) &= 2Y^p(n-1,m,k+1) - Y^p(n-2,m,k) \\ &\quad - \frac{1}{n}\Big[Y^p(n-1,m,k+1) - Y^p(n-2,m,k)\Big] \\ &= Y^p(n,m-2,k) + (2m-1)X^p(n,m-1,k+1) \end{aligned} \tag{A12}$$

initialized for all k by

$$\begin{aligned} Y^p(0,1,2k+1) &= \mathcal{I}(p+1,k+1) \\ Y^p(1,1,2k) &= \mathcal{I}(p+1,k+1) \end{aligned} \tag{A13}$$

c) The integrals of the third kind satisfy the recursion relations

$$\begin{aligned} Z^p(n,m,k) &= Z^p(n-2,m,k) + (2n-1)Y^p(n-1,m,k+1) \\ &= Z^p(n,m-2,k) + (2m-1)Y^p(m-1,n,k+1) \end{aligned} \tag{A14}$$

(note the inverted indexes in the second identity), initialized for all k by

$$Z^p(1,1,k) = \mathcal{I}(p+1,k+1) \tag{A15}$$

If toroidal trapping is taken into account as suggested in section 4, the recurrence relations (A10)-(A15) are still valid, but the integrals needed for the initialization have to be redefined by adding the factor $\mathcal{W}(\mu - \mu_{\rm cr})$ (eqn (20)) in the integrand. The integrals thus modified are not known in closed form, and must, therefore, be evaluated numerically on each magnetic surface, since $\mu_{\rm res}$ is a function of ψ. The oscillating nature of the integrands, moreover, makes it difficult to reach an accuracy comparable to that guaranteed when using the analytic expressions (A7). Since small errors in the initializations tend to be somewhat amplified by the recursion relations (10)-(15), convergence of the solution is often less satisfactory than when trapping effects are neglected.

[1] BRAMBILLA, M. and BILATO, R., Nuclear Fusion **46** (2006) S387.
[2] BRAMBILLA, M., Plasma Physics and Controlled Fusion **41** (1999) 1.
[3] WRIGHT, J. C., BONOLI, P. T., D'AZEVEDO, E., and BRAMBILLA, M., Computer Physics Communications **164** (2004) 330.
[4] BRAMBILLA, M., Nuclear Fusion **38** (1998) 1805.
[5] BRAMBILLA, M., Plasma Physics and Controlled Fusion **44** (2002) 2423.
[6] WRIGHT, J., BERRY, L., BONOLI, P., et al., Nuclear Fusion **45** (2005) 1411.
[7] BRAMBILLA, M., Nuclear Fusion **34** (1994) 1121.
[8] ERIKSSON, L.-G. and HELLSTEN, T., Phys. Scr. (Sweden) **52** (1995) 70.
[9] ERIKSSON, L.-G., HELLSTEN, T., and WILLEN, U., Nuclear Fusion **33** (1993) 1037.
[10] MANTSINEN, M. J., ERIKSSON, L.-G., BHATNAGAR, V. P., et al., Plasma Physics and Controlled Fusion **41** (1999) 843.
[11] DUMONT, R. J., PHILLIPS, C. K., and SMITHE, D. N., Physics of Plasmas **12** (2005) 042508.
[12] JAEGER, E. F., BERRY, L. A., AHERN, S. D., et al., Physics of Plasmas **13** (2006) 056101.
[13] JAEGER, E., HARVEY, R., BERRY, L., et al., Nuclear Fusion **46** (2006) S397.
[14] ERIKSSON, L.-G. and PORCELLI, F., Plasma Physics and Controlled Fusion **43** (2001) R145.
[15] FASOLI, A., GORMENZANO, C., BERK, H., et al., Nuclear Fusion **47** (2007) S264.
[16] HELLSTEN, T., CARLSSON, J., ERIKSSON, L.-G., HEDIN, J., and KÄLLBÄCK, J., Proceedings of 17th iaea fusion energy conference, in IAEA, editor, *Plasma Physics and Controlled Nuclear Fusion Research*, p. THP2/36, Yokohama, Japan, 1998, IAEA, IAEA.
[17] ERIKSSON, L.-G., MANTSINEN, M. J., HELLSTEN, T., and CARLSSON, J., Physics of Plasmas **6** (1999) 513.
[18] HEDIN, J., HELLSTEN, T., and ERIKSSON, L.-G., Nuclear Fusion **40** (2000) 1819.
[19] ERIKSSON, L.-G. and SCHNEIDER, M., Physics of Plasmas **12** (2005) 072524.
[20] STIX, T., Nuclear Fusion (1975).
[21] D.CONTE, B. and FRIED, S. D., *The Plasma Dispersion Function: the Hilbert Transform of the Gaussian*, Academic Press, 1961.
[22] VALEO, E. J., PHILLIPS, C. K., BONOLI, P. T., WRIGHT, J. C., and TEAM, M. B. R. S., Full-wave simulations of lh wave propagation in toroidal plasma with non-maxwellian electron distributions, in RYAN, P. M. and RASMUSSEN, D., editors, *RADIO FREQUENCY POWER IN PLASMAS: 17th Topical Conference on Radio Frequency Power in Plasmas*, volume 933, pp. 297–300, AIP, 2007.
[23] BENDANIEL, D. J. and ALLIS, W. P., Journal of Nuclear Energy. Part C, Plasma Physics, Accelerators, Thermonuclear Research **4** (1962) 31.
[24] KERBEL, G. D. and MCCOY, M. G., Computer Physics Communications **40** (1986) 105.
[25] DALLA, S. and LJEPOJEVIC, N. N., Physics of Plasmas **4** (1997) 2052.
[26] BRAMBILLA, M., Nuclear Fusion **47** (2007) 175.
[27] CATTO, P. J. and MYRA, J. R., Physics of Fluids B: Plasma Physics **4** (1992) 187.
[28] CATTO, P. J., MYRA, J. R., and RUSSELL, D. A., Physics of Plasmas **1** (1994) 52.
[29] BERNSTEIN, I. B. and MOLVIG, K., Physics of Fluids **26** (1983) 1488.
[30] HEIKKINEN, J. and SIPILA, S., Nuclear Fusion **37** (1997) 835.
[31] BRAMBILLA, M., *Kinetic Theory of Plasma Waves*, Oxford University Press, USA, 1998.
[32] BILATO, R., BRAMBILLA, M., PAVLENKO, I., and MEO, F., Nuclear Fusion **42** (2002) 1085.
[33] PRESS, W. H., TEUKOLSKY, S. A., VETTERLING, W. T., and FLANNERY, B. P., *Numerical Recipes 3rd Edition: The Art of Scientific Computing*, Cambridge University Press, 3 edition, 2007.